Applied Acoustics xxx (xxxx) xxx

Contents lists available at ScienceDirect

Applied Acoustics

journal homepage: www.elsevier.com/locate/apacoust

Influence of a micro-perforated duct absorber on sound emission and performance of axial fans

Felix Czwielong [a,*], Sebastian Floss [b], Manfred Kaltenbacher [b,c], Stefan Becker [a]

[a] Institute of Process Machinery and Systems Engineering, Friedrich-Alexander-University Erlangen-Nuernberg, Germany
[b] Institute of Mechanics and Mechatronics E325-3, TU Wien, Austria
[c] Institute of Fundamentals and Theory in Electrical Engineering, TU Graz, Austria

ARTICLE INFO

Article history:
Received 27 May 2020
Received in revised form 19 October 2020
Accepted 20 October 2020
Available online xxxx

Keywords:
Axial fans
Micro-perforated plate absorber
Duct modifications
Noise attenuation
Overflowed sound absorbers
Design optimization

ABSTRACT

In this article we investigate the influence of varying flow conditions on the acoustic behaviour of a micro-perforated panel absorber (MPA), applied in the vicinity of an axial fan. The predesign of the MPA was conducted by using the Finite Element Method (FE) in combination with porous material modelling approaches. Experimental results of emitted sound spectra and fan characteristic of different fan blade geometries, positioning of the fan to the absorber, as well as changes in turbulent intensity are presented. The studies showed that the investigated MPA duct reduces the overall sound pressure level emitted by the fan by up to 16 dB while maintaining the same efficiency and pressure build-up. From an acoustic and aerodynamic point of view, it was more efficient if the fan operate downstream of the MPA instead of within the MPA. This arrangement increased the efficiency and avoided high-frequency sound generation, which is caused by the flow through the MPA. The results show that the function of the MPA can be used for different fan geometries and that inlet turbulence improves the properties of the absorber.

© 2020 Elsevier Ltd. All rights reserved.

1. Introduction

Axial fans are one of the most common machines used in the field of cooling and air-conditioning technology. The task of the axial fan is to provide a volume flow which is either used for the removal of process heat or to supply rooms with fresh air. Axial fans are used, for example, in heat pumps, air conditioning systems, exhaust systems in buildings, computers, chemical plants and vehicles [1–7]. All these applications are in the direct vicinity of humans, which means that high standards are set for the comfortable operation of the machines. The axial fan is becoming more and more important in terms of acoustic optimization, so that less noise pollution for people can be guaranteed. Several studies have already shown that it is possible to modify the blades of the axial fan in such a way that they induce a lower noise emission. For example, it has been found that a forward-skewed fan has a lower sound emission than unskewed or backward-skewed fans when the airflow is not disturbed [8–11]. Modifications to the leading edge with sinusoidal serrations, slits or porous materials have also been investigated and have led to a reduction in the sound pressure level [12–16]. However, in most cases such direct noise reduction measures also have an effect on the aerodynamic properties of the fan. For example, if the modifications are not precisely adapted to the flow field of the fan, a lower sound pressure level may be achieved, but the pressure build-up and thus the efficiency of the fan will also decrease [16–18]. A lower pressure build-up would therefore have to be compensated by an increased speed, which in turn leads to a higher sound pressure level. Since the sound pressure level of the fan is speed-dependent, a higher sound pressure level can be achieved with the same pressure increase despite modification [19]. Axial fans often operate in ducts and are part of systems consisting of several components such as protective grids, heat exchangers, filters, etc., the fans rarely operate under undisturbed inflow conditions. Disturbed inflow conditions affect the aerodynamics and acoustics of the fans and in most cases lead to higher sound radiation [20–23]. Also the effects of direct noise reduction measures on the fan such as fan blade skew or leading edge modification can change under disturbed and more turbulent inflow conditions. Such effects have already been investigated by Krömer [11] and Biedermann [18,24] on generic turbulence grids. According to this, forward-skewed fans react more sensitively to disturbed inflow conditions. Modifications of the leading edge achieve better noise reduction properties under disturbed inflow conditions. In addition to the direct noise reduction measures,

* Corresponding author.

https://doi.org/10.1016/j.apacoust.2020.107746
0003-682X/© 2020 Elsevier Ltd. All rights reserved.

Please cite this article as: F. Czwielong, S. Floss, M. Kaltenbacher et al., Influence of a micro-perforated duct absorber on sound emission and performance of axial fans, Applied Acoustics, https://doi.org/10.1016/j.apacoust.2020.107746

Nomenclature

D_{MPP}	Duct diameter of MPP duct
$D_{c,max}$	Maximum of Cavity depth
D_c	Cavity depth
D_{duct}	Duct diameter
D_{fan}	Total fan diameter
D_{hub}	Hub diameter of the fan
L_{Slits}	Length of slits on MPP
L_c	Cavity length
L_c	Length of duct section
L_p	Sound pressure level
M_s	Torque offset
R_a	Outer radius of the duct
R_{mic}	Radius of the microphone setup
S_{grid}	Distance turbulence grid to inlet nozzle
S_{tip}	Tip gape size of the fan
T_{bar}	Bar width of turbulence grid
T_{cl}	Turbulence grid clearance
T_m	Turbulence grid mesh size
W_{Slits}	Width of slits on MPP
Z_{blades}	Number of fan blades
Φ_{mic}	Angle between microphones
$\dot{V}$	Volume flow rate
$\dot{V}_{fan}$	Design volume flow rate of the fan
$\dot{n}_{fan}$	Design rotational speed of the fan
λ	Wavelength
λ_{fan}	Sweep angle of fan blades
ϕ_{MPP}	Perforation rate of MPP
σ	Turbulence grid solidity
f	Frequency
f_{BPF}	Blade Passing Frequency of the fan
f_c	Cut-off Frequency
f_{samp}	Sampling frequency
p^+	Incident sound wave
p^-	Returning sound wave
p_{ts}	Total-to-static pressure difference
s_{MPP}	Thickness of MPP
s_{raw}	Thickness of MPP raw material
t_{samp}	Measuring time
V	Volume of the anechoic chamber
B	Backward skewed axial fan
BPF	Blade passing frequency
CAD	Computer-aided design
CFS++	Coupled field simulation
F	Forward skewed axial fan
M5FS	Short MPA duct (500 mm diameter) with free inflow
MFL	Long MPA duct with free inflow
MFS	Short MPA duct with free inflow
MPA	Micro-perforated Absorber
MPP	Micro-perforated Panel
MTL	Long MPA duct with turbulence grid
MTS	Short MPA duct with turbulence grid
NACA	National Advisory Committee for Aeronautics
RFL	Long reference duct with free inflow
RFS	Short reference duct with free inflow
RTL	Long reference duct with turbulence grid
RTS	Short reference duct with turbulence grid

which take place at the fan blades, passive measures can also be implemented. Passive measures are, for example, sound absorbers which are inserted into the duct system. In most cases, however, these measures lead to an additional pressure loss in the system [25,26]. These can lead to further problems if sound absorbers made of classic foams are used. These materials can be partially flammable, accumulate toxic and harmful substances and pose a danger to humans due to the smallest fibers that are carried along by the air flow. Micro-perforated panel absorbers (MPA), which can be made of glass, aluminum, stainless steel or plastic, do not have the disadvantages of classic porous sound absorber materials. So most MPA are stable against mechanical effects, fireproof, fiber-free, easy to clean, chemically resistant and can be used for flow guidance due to their high flow resistance. These advantages of MPAs are particularly important when a high level of comfort and safety for people is required, which is the case, for example, with air conditioning systems and HVAC systems where people are in direct contact with the fluid flow from the entire duct-turbomachinery-silencer system [27–31]. Additional benefit can be provided by micro-perforated sound absorbers if they are used as circular walls of ducts and no additional central body is used for additional sound reduction. Due to the high flow resistance of the MPA, this arrangement results in a flow guidance which is associated with only a small additional pressure loss. Due to the low pressure loss, high efficiency of the complete duct system can be combined with low noise emission [26,28]. MPAs have so far been investigated in a large number of studies, the majority of which, however, refer to the absorbers being located in a quiescent environment without flow [32–35]. Cases with grazing flow have been investigated by Allam [36], for example, who used the MPP for the casing of splitter typ silencers. The effect of air flow over an expansion chamber based MPA in direct vicinity to a fan on its noise reduction has only been investigated to date by Dong et al. [31]. Circular pore MPPs were applied on a contra-rotating fan. They were able to show that relatively large submillimeter pore diameters provide effective sound absorption in the 1 to 2 kHz regime in small-scale scenario due to manufacturing constraints. A minor influence of the MPP casing on overall pressure loss could be confirmed. In addition, no studies have been carried out on how disturbed inflow conditions affect the interaction with the absorber. Nonlinear effects due to bias flow, grazing flow or large sound pressure amplitudes on the acoustic behavior of MPPs with circular perforations have been investigated Temiz [37], Zhang [38] and Lawn [39]. In each case the investigations were either limited to simulated isolated pores or impedance tube measurements showing an increased resistive part of the MPP pore impedance with increased grazing or bias flow. In this study slitted micro-perforated absorbers are used in a modified version for a large scale application scenario with the aim of placing the fan in direct vicinity of the MPA. The fan running above the absorber would allow more absorber area in a limited space scenario. The round duct of the axial fan is replaced by a duct which is lined with micro-perforated panels (MPP). A cavity is created behind these panels, which acts as an absorber together with the micro-perforated panel. Due to this modified version, the flow is influenced as less as possible and at the same time the noise reduction is high. The aim of this thesis is to determine the influence of micro-perforated absorbers in the direct vicinity of axial fans. On the one hand the aerodynamic and on the other hand the acoustic interactions are considered. In addition, it is to be investigated how different skewed fan blades and different inflow conditions with different turbulent kinetic energies affect the aerodynamics and acoustics of the entire system (micro-perforated absorber and axial fan).

2. Micro-perforated absorber and axial fans

2.1. Micro-perforated panel and cavity

In this study the influence of a micro-perforated absorber is investigated. This sound absorber consists of two components, a micro-perforated panel (MPP) and a back volume behind it called cavity. The selection of length of the cavity allows to target high absorption in specific frequency bands. In the presented case frequencies below 500 Hz to cover the first blade passing frequency $f_{\mathrm{BPF}} = 222$ Hz of the investigated fans. On the other hand the cavity length should be as small as possible due to space limitations. Also, the absorber structure should not act as an obstruction to the flow which would have a detrimental effect on the overall pressure drop. Fig. 1 schematically shows the basic structure of the sound absorber used. The sound energy of incoming sound waves is dissipated in the openings of the MPP, which are in the sub-millimeter range. The back wall of the cavity is designated as a sound hard wall and is located at distance D_c from the MPP. By setting the distance D_c, specific frequencies at which maximum absorption takes place can be set. Usually the distance D_c is selected as $\lambda/4$ of the target wavelength λ. By choosing this arrangement, a maximum of the particle velocity is located directly within the MPP which leads to a high dissipation. In addition to the influence of the MPP, the cavity exerts an impedance jump due to its cross-sectional change, which leads to a sound reduction. By reflection at the axial length of the MPA, especially low frequencies can be reduced [35,40–44].

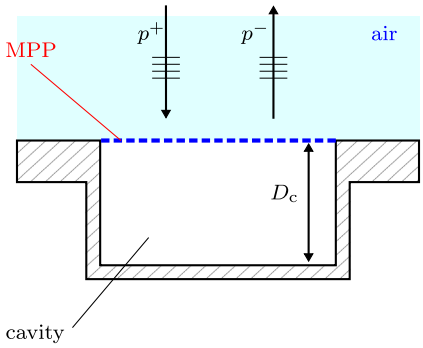

Fig. 1. Schematic representation of a micro-perforated absorber (MPA) made of a micro-perforated panel (MPP) and a cavity filled with air [41].

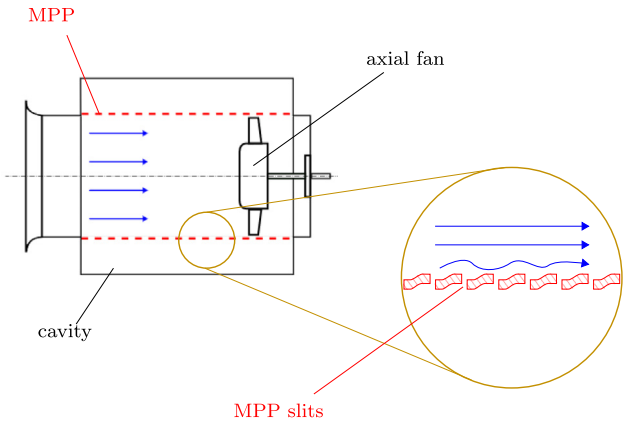

Fig. 2. Schematic representation of the MPA designed as a duct, whereby the MPP is used to guide the flow.

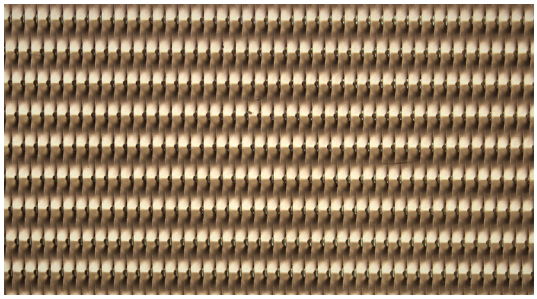

Fig. 3. Close-up photography of the installed micro-perforated panel (SONTECH, *Acustimet*™) with pores designed as slits.

Table 1
Parameters of MPA.

MPA parameter	Value
Cavity length L_c	440 mm
Cavity depth D_c	137 mm
MPP duct diameter D_{MPP}	506 mm
MPP thickness raw material s_{raw}	0.5 mm
MPP thickness s_{MPP}	≈1.2–1.6 mm
MPP perforation rate ϕ_{MPP}	1%
MPP pores	slits
MPP producer	SONTECH
Slits length L_{slits}	2 mm
Slits width W_{slits}	0.074 mm

Behind the MPP duct there is a continuous back volume, which is designed as an octagon shape and surrounds the MPP duct. The investigated MPP, provided by SONTECH (*Acustimet*™), are made of stainless steel with a thickness of s_{MPP} and the pores are designed as slits (see schematic in Fig. 2). A close-up photography of the MPP's slit arrangement is shown in the Fig. 3. This variant of MPP was chosen because it is commercially available and cheap in production. The material is only plastically deformed by rolling semi-finished aluminum plates [27,30]. The most important design parameters of the MPA are summarized in the Table 1. The MPP parameters were determined as described in [44] by fitting impedance tube measurements to transfer function model based on Johnson-Champoux-Allard-Lafarge (see [45] for details). These effective material parameters were used in the Finite Element based research software CFS++ [46]. The usage of non-conforming grid techniques [47] facilitated a parameter study to determine cavity length L_c and an optimal cavity depth D_c with the constraint of maximum $D_{c,\max} = 200$ mm. Effectively, the real material's acoustic behavior was mimicked by an equivalent fluid volume with the same absorption behavior by using fitted parameters for porosity and hydraulic radius. The matching procedure was carried out by a non-linear least-squares algorithm in the Matlab toolbox. The value for porosity in Table 1 was provided by the manufacturer and is obtained by light transmission measurement. The slit length and width were measured at the institute. The measured parameters of the micro-perforated plate are associated with a certain degree of uncertainty due to the complex slit geometry. Nevertheless, established impedance models, like Maa's, require precise input data.

2.2. Axial fans

The influence of the MPA on the noise emissions of axial fans is investigated on two different fans. The two fans are identical and differ only in the fan blade skew. Thus a backward skewed fan with the sweep angle of $\lambda_{\mathrm{fan}} \in [0°; -55°]$ and a forward skewed fan with

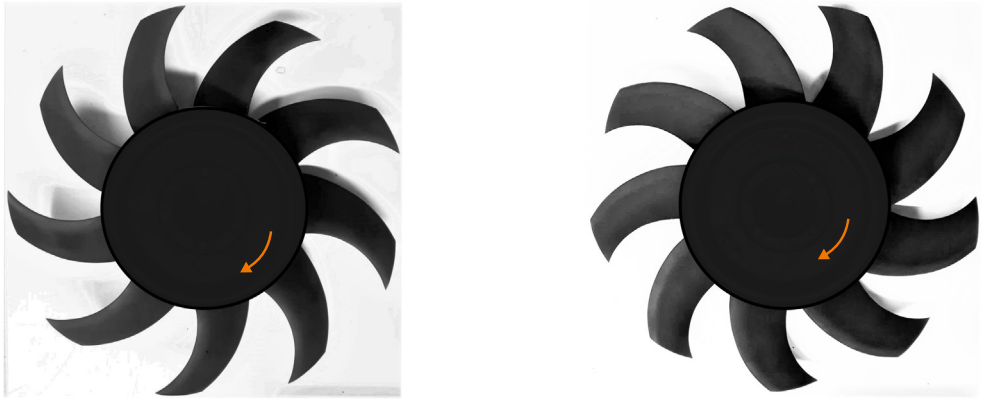

(a) forward skewed fan (F) (b) backward skewed fan (B)

Fig. 4. Photography of the axial fans, (a) fan F with forward skewed fan blades and (b) fan B with backward skewed blades.

Table 2
Design parameters of the axial fans.

Parameter	Value
Number of fan blades Z_{blades}	9
Total fan diameter D_{fan}	495 mm
Duct diameter D_{duct}	500 mm
Hub diameter D_{hub}	247.5 mm
Tip gap size S_{tip}	2.5 mm
Design volume flow $\dot{V}_{fan}$	1.4 m^3s^{-1}
Design speed n_{fan}	1486 min^{-1}
NACA-profile	NACA 4510 [54]

sweep angle of $\lambda_{fan} \in [0°; 55°]$ are investigated. A sweep angle of $\lambda_{fan} = 0°$ is applied to the hub of both fans. This sweep angle changes its value linearly over the span of the blade. The fans used are shown in the Fig. 4. These two fans were chosen because there is a large database of aerodynamic and acoustic properties of the two fans in the literature [11,10,21,48,49]. Furthermore, backward and forward skewed fans are frequently used in technical systems.

The axial fans were designed according to the blade element theory [19,50,51]. Both of them have $Z_{blades} = 9$ blades and are configured for optimal operation for a volume flow rate of $\dot{V}_{fan}$ = 1.4 m^3s^{-1} and a rotational speed of n_{fan} = 1486 min^{-1}. The most important dimensions of the fans are listed in the Table 2.

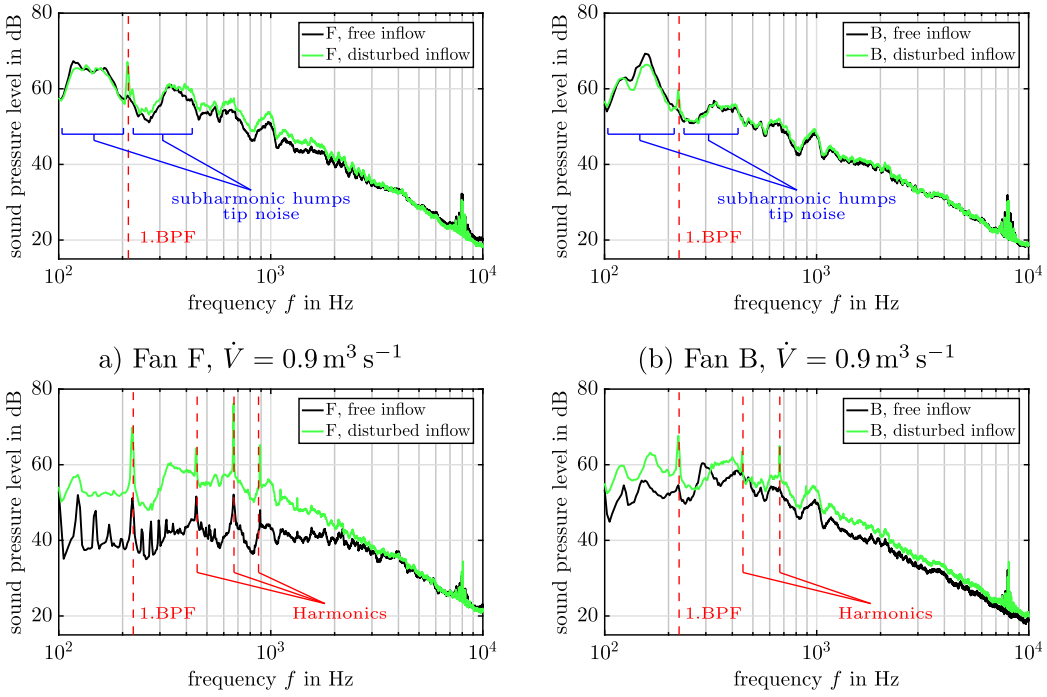

a) Fan F, $\dot{V} = 0.9\,m^3\,s^{-1}$ (b) Fan B, $\dot{V} = 0.9\,m^3\,s^{-1}$

(c) Fan F, $\dot{V} = 1.4\,m^3\,s^{-1}$ (d) Fan B, $\dot{V} = 1.4\,m^3\,s^{-1}$

Fig. 5. Averaged sound pressure spectra of fans F (a and c) and B (b and d) operating in a short duct with different inlet turbulence at the design point ($\dot{V}$ = 1.4 m^3s^{-1}) and in the part load range ($\dot{V}$ = 0.9 m^3s^{-1}). Red dashed lines indicate the blade passing frequency (BPF) and its harmonics. The areas in blue brackets represent the subharmonic humps in the spectrum, which mainly occur in the partial load range and are caused by the interaction of the leading edge of the blade with the vortex structures in the tip gap of the fan.

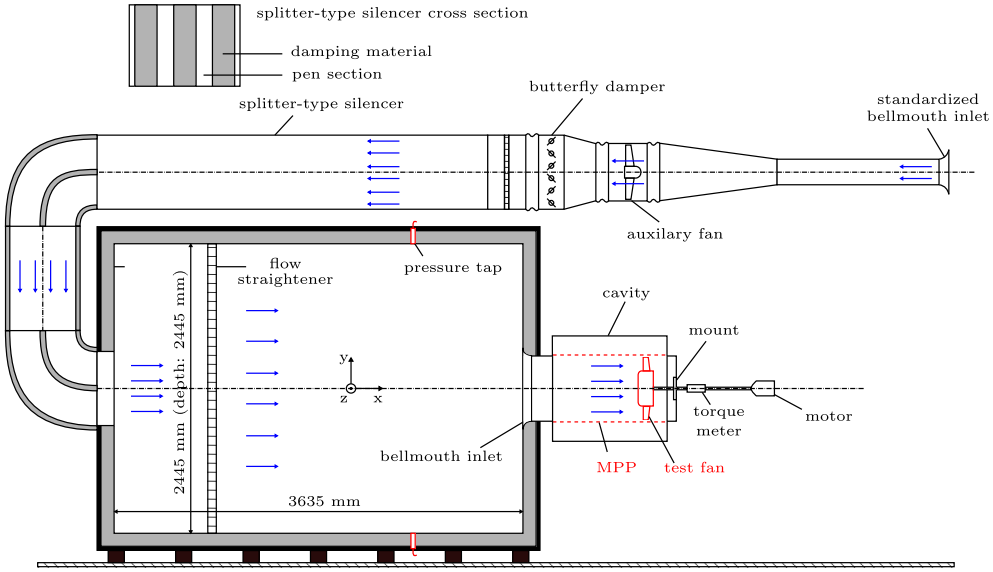

Fig. 6. Standardized inlet test chamber according to ISO 5801 [55] with micro-perforated absorber (MPA) duct (micro-perforated panel (MPP) and cavity) and axial test fan.

The behaviour of the two fans has already been experimentally examined in several studies. It was found that at the design point the forward skewed fan is the quieter version of the two fans. In addition, the backward skewed fan showed higher sound sources, which are due to the interaction of the blade tips with the tip gap flow. The forward skewed fan was found to be more sensitive to disturbed inflow conditions [11,21,23]. Fig. 5 shows the sound pressure spectra of the used fans for free and turbulent inflow operating in a short duct at two different operation points (part load range $\dot{V}$ = 0.9 m^3s^{-1}, design point $\dot{V} = 1.4$ m^3s^{-1}). The increased turbulence was generated with a turbulence grid upstream of the fans. From the spectra shown, the acoustic properties of the fans can be identified. In the partial load range (see Fig. 5 (a) and (b)) subharmonic components are visible in the spectra, which are caused by the formation of coherent flow structures in the tip gap and interact with the leading edge of the fan. These sound sources are usually amplified with increasing tip gap [52,11]. Furthermore, these sound sources are influenced by the operating point of the fan and the blade shape. For example, it can be seen that this sound mechanism for the backward skewed fan is still present in the region of the design point, whereas this is not the case for the forward skewed fan (see Fig. 5(c) and (d)). The tonal components of the fans used are more pronounced from the design point onwards. These are increased by turbulent inflow for both fans. In addition, turbulent inflow leads to an increase in broadband sound up to $f = 3$ kHz for these fans (leading edge sound). It can be seen that the forward skewed fan reacts much stronger to the changed inflow than the backward skewed fan at the design point. With their different characteristics, these two fans are particularly suitable for obtaining a general applicability of the results. The acoustic properties shown can change further with varying duct lengths, because these affect the inflow and acoustic propagation of duct modes [11,53].

Table 3
Parameters of turbulence grid.

Parameter	Value
Bar width T_{bar}	16 mm
Clearance T_{cl}	80 mm
Mesh size T_m	96 mm
Solidity σ	0.31

3. Experimental setup

3.1. Inlet test chamber for axial fans

The experimental investigations were carried out in an axial fan test rig standardised according to DIN EN ISO 5801 [55]. The test rig has a anechoic chamber on the suction side of the test axial fan, which makes it technically possible to determine the sound emissions of the fan. A cross-section of the inlet test rig is shown in Fig. 6. The air is drawn in through a standardized inlet nozzle. The volume flow is determined via this nozzle. For the adjustment of the operating point the test stand has an auxiliary fan and a butterfly throttle. Before the air enters the anechoic chamber, it is made quiet by splitter-type silencers. The anechoic chamber on the suction side of the axial fan has a volume of $V = 22$ m^3 and has a quiescent sound pressure level $L_p = 28$ dB for the frequency range of $f \in$ [0.1 kHz;10 kHz]. The walls of the chamber are built in a sandwich structure, which consists of 80 mm thick acoustic foam, 20 mm acoustic heavy foam and 2.5 mm acoustic heavy foil inside. These are mounted on acoustic sound insulation panels. The cut-off frequency of the anechoic chamber is $f_c = 254$ Hz and has reverberation times in the range of [0.03 s;0.19 s]. Just before the inlet nozzle of the axial fan there is a ring pressure tap which is connected to a differential pressure sensor (Setra, type 2391-500LB-1F-2B-02-9-NN) with the ambience to measure the total-to-static pressure difference p_{ts} of the fan. The pressure sensor has a measurement inaccuracy of $\pm 0.073\%$ on the measured value. The inlet nozzle of the fan is connected to the test bench wall. The duct in which the fan operates is variable so that the length can be changed. At a distance of $S_{grid} = 220$ mm from the inlet nozzle it is possible to insert generic turbulence grids into the flow. Numerous studies on the induced flow field of the used turbulence grid can be found in the literature [10,11,48]. The characteristic data of the grid are shown in Table 3. After the turbulence grid a replaceable duct section is located. This duct section has a length of $L_c = 440$ mm and represents in the reference variant a straight duct with the diameter $D_{duct} = 500$ mm. In the second variant this duct section is replaced by a micro-perforated duct. The micro-perforated duct has the properties described in chapter 2. The circular mirco-perforated absorber is equipped with a back volume, which can be changed by different installations. Thus the back volume can be divided in azimuth and radial direction. In addition,

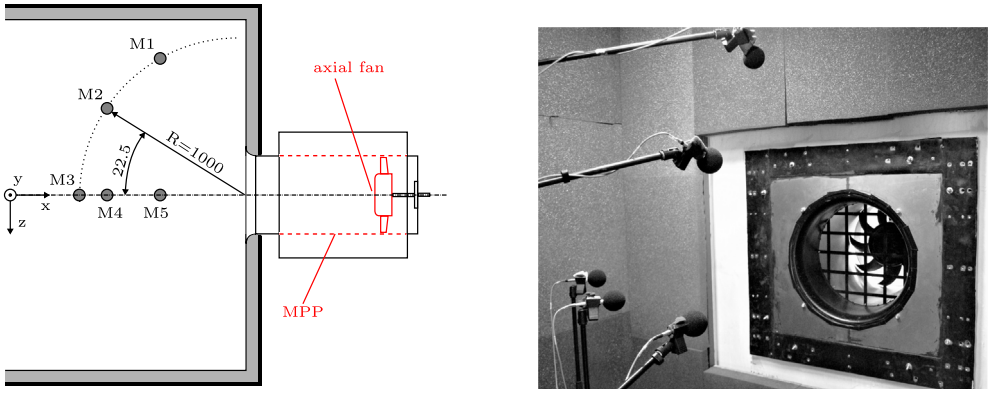

(a) microphone positions (b) photo of the test setup

Fig. 7. Representation of the experimental setup for characterization of the sound field, (a) schematic drawing with microphone positions (M1-M5) and (b) photo of the experimental setup with installed turbulence grid.

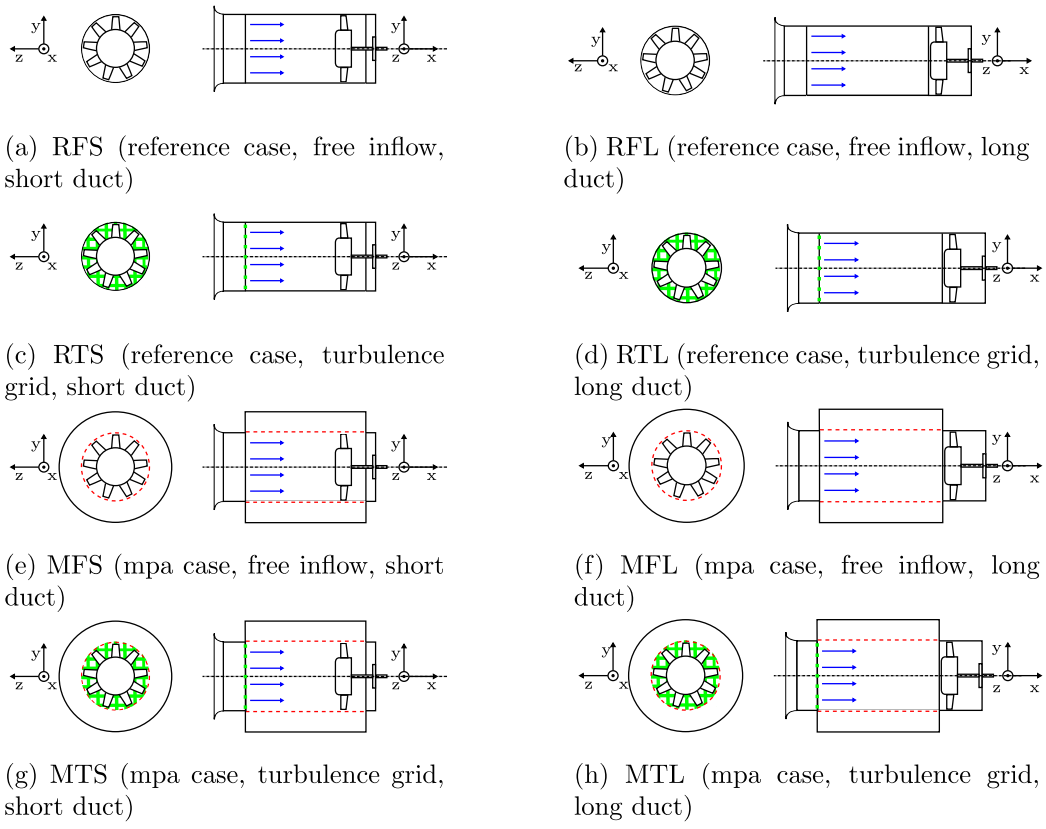

(a) RFS (reference case, free inflow, short duct)

(b) RFL (reference case, free inflow, long duct)

(c) RTS (reference case, turbulence grid, short duct)

(d) RTL (reference case, turbulence grid, long duct)

(e) MFS (mpa case, free inflow, short duct)

(f) MFL (mpa case, free inflow, long duct)

(g) MTS (mpa case, turbulence grid, short duct)

(h) MTL (mpa case, turbulence grid, long duct)

Fig. 8. Schematic representations of the investigated duct setups, in red the MPP, in green the turbulence grid. The reference duct is marked with R and the MPA duct with M. The free flow is indicated by F, the turbulent flow with turbulence grid is marked with T. The long duct is labeled with L and the short one with S.

inserts such as liners can also be inserted into the cavity. The diameter of the micro-perforated tube is $D_{MPP} = 500$ mm and thus slightly larger than the standard reference duct. Depending on the variant, the examined axial fan is operated directly in the perforated duct or shortly downstream in an unperforated duct section. The fan is supported by 4 non-centric support struts, which lower the rotor-stator-interaction [11]. Outside the duct is the motor drive unit. This is equipped with a torque and speed sensor (burster, typ 8861), so that the power and efficiency of the fan can be determined. The measurement uncertainty of the torque sensor is 0.1% on the measured value. The torque values of the fan are corrected with a predetermined torque offset M_s, which includes momentum due to bearing friction. For more detailed information on the test rig and the turbulence grid used, please refer to the literature [11,17,21].

3.2. Experimental setup for the sound emissions

The radiated sound field of axial fans is determined on the suction side of the turbomachinery. For this purpose five free-field microphones (Brüel & kJær, type 4189-L-001) with preamplifier (Brüel & kJær, type 2669-L) are used within the anechoic chamber. The microphones are connected to a microphone amplifier (Brüel & kJær, type Nexus 2690-A) and are calibrated with a microphone

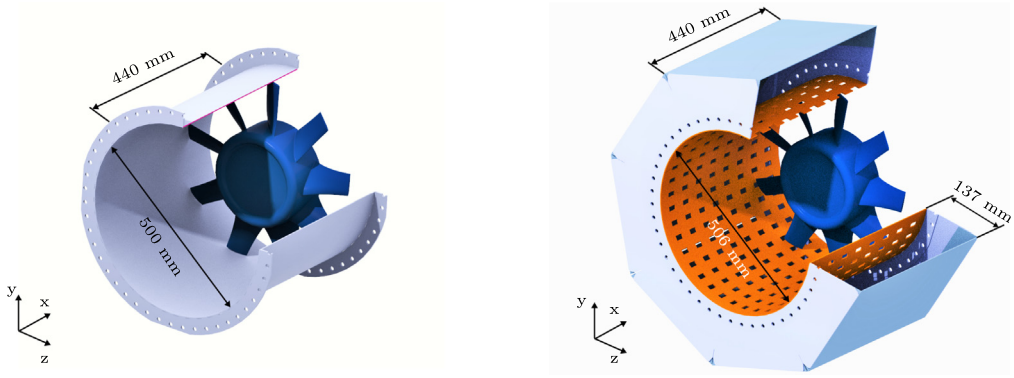

Fig. 9. CAD representation of the RFS (a) and MFS (b) cases.

calibrator (Brüel & kJær, type 4231) before measurement. A PXIe-1075 front-end (NI) chassis with a high-precision 24-bit PXIe-4492 (NI) data acquisition module was used to acquire the measurement data. The components of the measurement technology were controlled by the software LabView (NI). The microphones used have a free field response of ±1 dB over the frequency range of $f \in [10\,\text{Hz};8\,\text{kHz}]$ and the microphone preamps of ±0.5 dB over the frequency range of $f \in [3\,\text{Hz};200\,\text{kHz}]$. The microphones are all located at a distance of $R_{\text{Mic}} = 1000$ mm from the fan inlet bell-mouth. The arrangement of the microphones is shown schematically in Fig. 7(a) and (b) shows a photograph of the experimental setup with built-in turbulence grid and forward skewed fan. One microphone (M3) is located on the rotation axis of the fan and two microphones (M1-M2) are located on a horizontal quarter circle to the rotation axis of the fan. The microphones (M3-M5) are arranged on a vertical quarter circle. The angle segments between the individual microphones are each $\Phi_{\text{Mic}} = 22.5°$. As soon as a stable operating point is reached, the sound pressure is measured parallel to the determination of the aerodynamic characteristics of the fan. The sound pressure is measured for a measuring time of $t_{\text{samp}} = 30$ s with a sampling frequency of $f_{\text{samp}} = 48$ kHz. The resulting sound pressure level spectrum is calculated from the energetically averaged sound pressure of all five microphones (M1-M5). The total sound pressure level of each measurement is calculated from the average sound pressure spectrum for the frequency range of $f \in [0.1\,\text{kHz};10\,\text{kHz}]$. For details we refer to [11,21].

3.3. Investigated duct setups

In this study, different duct designs are investigated. In addition to the interactions of the fan with the absorber, these should also clarify how the position of the absorber in relation to the fan and inflow turbulence affect the sound radiation and fan efficiency. The various duct setups are shown in Fig. 8(a)–(h). Here a short duct system (a) and a long duct system (b) are analysed. In these two variants, on the one hand the fan operates with in the MPA duct section (Fig. 8(e) and (g)) and on the other hand it operates downstream of the MPA (Fig. 8(f) and (h)). In both cases the active absorber surface is kept the same. A further case is the change of the inflow conditions. In addition to the free inflow, it is investigated how a more turbulent inflow affects the absorber and the fan. The turbulent inflow is generated by means of a turbulence grid, which is located in front of the absorber (Fig. 8(c) and (d)). The influence is investigated in both the long and the short duct system, but only for the forward-skewed fan. The four described duct setups exist on the one hand as reference case (standard duct) and on the other hand as MPA variant (Fig. 8(e)–(h)). In the MPA variant, one duct segment was replaced by the previously described MPA duct. In addition to the variants described here, there is a test case in which a modified MPP was inserted into the MPA absorber. The MPPs have the same properties, but the diameter of the duct has been reduced so that it has a value of $D_{\text{M5FS}} = 500mm$. This modified MPA sound absorber will be referred to as M5FS in the following, where 5 indicates the diameter. For a round duct with the outer radius of $R_a = D_{\text{duct}}/2 = 250$ mm, the cut-off frequency of the first circumferential mode is $f_c = 402$ Hz. For the extended duct (with cavity) with the outer radius is $R_a = 387$ mm and the cut-off frequency drops to $f_c = 259.7$ Hz [19].

Fig. 9 shows the case RFS and MFS as CAD. In the reference case displayed in Fig. 9(a) the fan is located in a standard duct. This duct is replaced for the investigations with a MPA duct (Fig. 9(b)). This consists of the MPP (shown in orange) and a back volume, which has an octagonal geometry. In Fig. 9(b) the slits of the MPP are shown enlarged, in reality their dimensions are in the sub-millimeter range.

4. Sound reduction in dependence of different boundary conditions

4.1. Influence of the tip gap clearance dimensions

The actual investigations, which are intended to find out what influences a duct consisting of MPA has on the acoustics and aerodynamics of axial fans, were carried out with an MPA duct which has a slightly larger diameter than the reference duct ($D_{\text{MPP}} = 506$ mm $> D_{\text{duct}} = 500$ mm). This has the consequence that the tip gap flow of the fan is affected and due to increased backflow from the pressure to the suction side of the fan the efficiency and pressure jump of the fan changes. In addition, the sound sources in the tip gap of the fan are dominant sound sources, which occur mainly in the subharmonic range between the tonal peaks of the blade passing frequency. These sound sources are amplified due to the larger tip gap. The sound sources in the tip gap are particularly important in the unsteady operating range of the fan, i.e at low volume flow rates [11,52,56]. In order to consolidate the basic findings of the investigations and to determine the influences of the different tip gaps between the MPA duct and the reference, another MPA duct was manufactured for one test case. This has the same properties as the actual MPA duct, only that the duct diameter is identical to the diameter of the reference duct

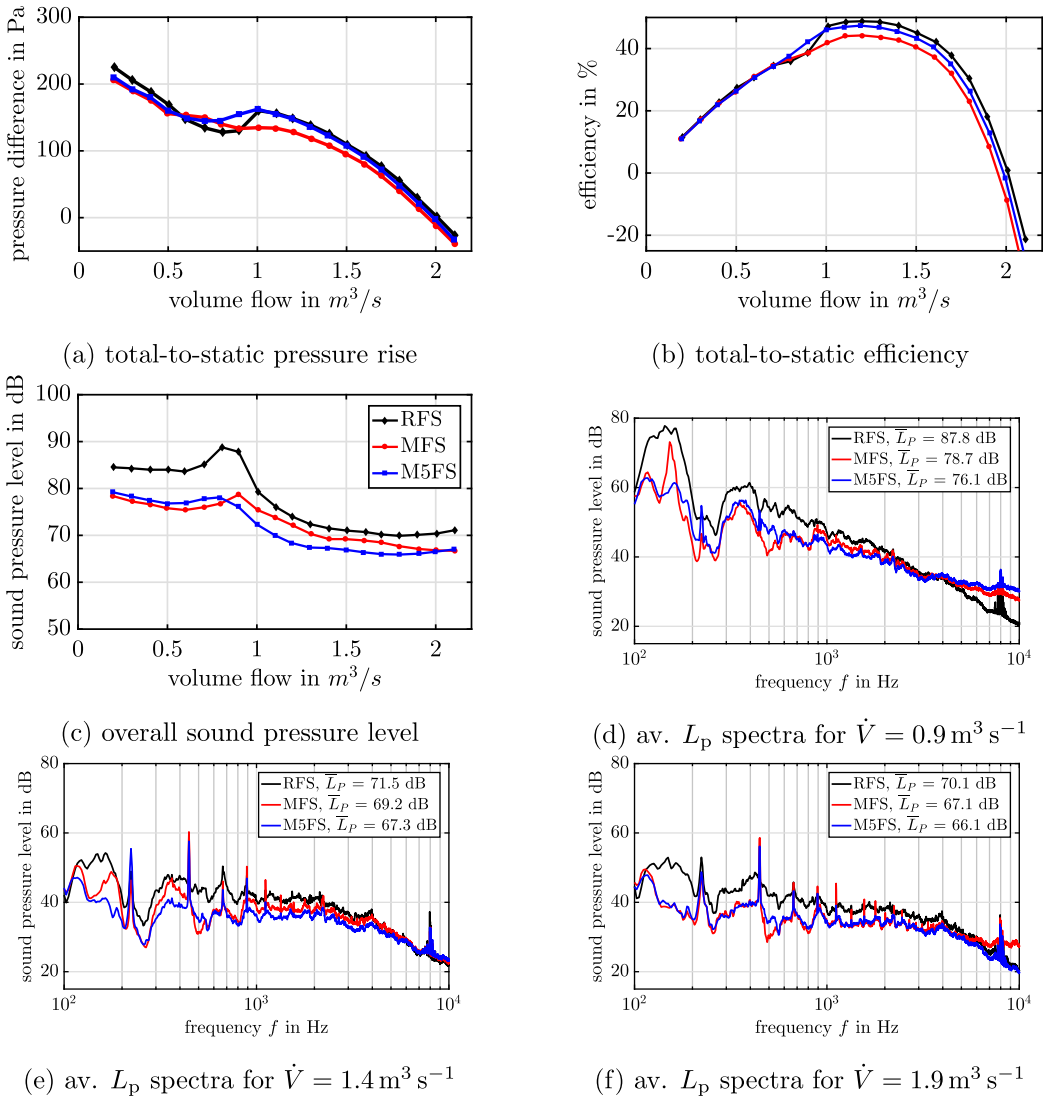

(a) total-to-static pressure rise

(b) total-to-static efficiency

(c) overall sound pressure level

(d) av. L_p spectra for $\dot{V} = 0.9\,\mathrm{m^3\,s^{-1}}$

(e) av. L_p spectra for $\dot{V} = 1.4\,\mathrm{m^3\,s^{-1}}$

(f) av. L_p spectra for $\dot{V} = 1.9\,\mathrm{m^3\,s^{-1}}$

Fig. 10. Results of the measurements for the varying tip gap.

($D_{\mathrm{M5FS}} = 500$ mm $= D_{\mathrm{duct}} = 500$ mm). Fig. 10 shows the results for the comparison between reference duct (RFS), MPA duct (MFS) and MPA duct with corrected diameter of $D_{\mathrm{M5FS}} = 500$ mm (M5FS). The cases were carried out with undisturbed inflow in the short duct system with the forward skewed fan.

The aerodynamic curves (Fig. 10(a)) show that due to the MPA duct the pressure difference of the fan decreases. Only in the non-stationary range of $\dot{V} \in n\,[0.6\ \mathrm{m^3 s^{-1}};\ 0.9\ \mathrm{m^3 s^{-1}}]$ the pressure difference generated by the fan increases. Comparing the measured pressure difference of the M5FS duct, it is noticeable that the pressure difference of $\dot{V} \in [1.0\ \mathrm{m^3 s^{-1}};\ 2.0\ \mathrm{m^3 s^{-1}}]$ is almost identical to that of the reference duct. This indicates that the reduced pressure difference of the fan is a cause of the different tip gap (MFS) and is not caused by the MPA. Also in the case of the suitable duct diameter (M5FS), the pressure difference generated has increased in the range $\dot{V} \in [0.6\ \mathrm{m^3 s^{-1}};\ 1.0\ \mathrm{m^3 s^{-1}}]$ compared to the reference duct. The efficiency curve (Fig. 10(b)) also reflects the decreased efficiency due to the increased tip gap in the MFS case. The efficiency with adapted diameter (M5FS) approaches the efficiency with respect to the reference case, which is 2% lower. The reduced efficiency could be due to the fact that the boundary layer in the tip gap is increased due to the rough surface of the MPA and the fan needs a higher torque to be driven due to the increased impulse exchange in the boundary layer. In the same way, an increased backflow through the pores of the MPP could explain the small difference in pressure build-up and be a cause for the reduced efficiency. The acoustic characteristics (Fig. 10(c)) show that the sound pressure level emitted by the fan can be significantly attenuated by the MPA duct. With a suitable tip gap (M5FS) this effect is even more significant, so that reductions of up to $\Delta L_\mathrm{p} = 4$ dB can be achieved for the total sound pressure level at the volume flow rate of $\dot{V} = 1.4\ \mathrm{m^3 s^{-1}}$. The greatest reductions occur for small volume flows. In this region, the tip gap flow and the associated sound sources are particularly significant [11,52,56]. The reductions in the sound pressure level take on values up to $\Delta L_\mathrm{p} = 10$ dB in this region. The differences due to the larger tip gap in the MPA duct (MFS) occur mainly in the volume flow range of $\dot{V} \in [0.8\ \mathrm{m^3 s^{-1}};\ 1.9\ \mathrm{m^3 s^{-1}}]$. In this range the sound pressure level is up to $\Delta L_\mathrm{p} = 3$ dB higher due to the increased tip gap. In principle, however, the damping properties of the MPA duct (MFS) are present.

The sound pressure spectra (Fig. 10(d-e)) show that the sound pressure of the subharmonic humps is more pronounced in the MFS case than in the M5FS case. This is the effect of the increased tip gap. In addition, the tonal components due to the blade passing

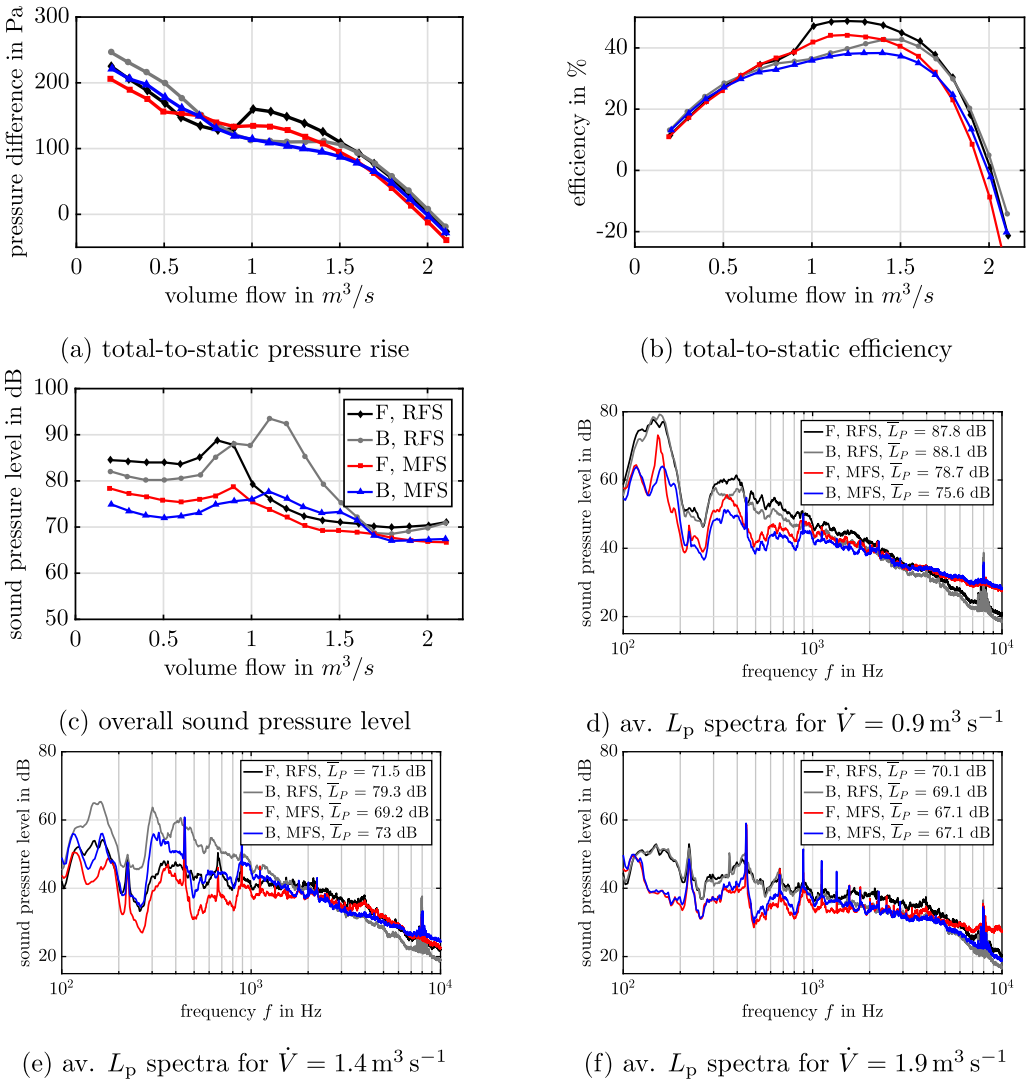

(a) total-to-static pressure rise

(b) total-to-static efficiency

(c) overall sound pressure level

d) av. L_p spectra for $\dot{V} = 0.9\,\mathrm{m^3\,s^{-1}}$

(e) av. L_p spectra for $\dot{V} = 1.4\,\mathrm{m^3\,s^{-1}}$

(f) av. L_p spectra for $\dot{V} = 1.9\,\mathrm{m^3\,s^{-1}}$

Fig. 11. Aerodynamic and acoustic results for the comparison between the fans F and B in the short duct.

frequency are increased in the MFS case. This could be related to the weld seam of the round MPP duct MFS, which, due to industrial fabrication, comes up against certain limitations of surface quality. The MPA duct consists of a plate of MPP, which is bent and then welded or glued to maintain the round shape of the duct. This weld seam is worse in the case of MFS than in the case of M5FS. These disturbances increase the turbulence of the flow locally, which in turn increases the unsteady forces on the blades. As a result, the sound pressure level at the blade passing frequency is increased [57–59]. On the basis of the results presented all basic effects become apparent with the case MFS, although it has a slitly larger duct diameter. For a case with a suitable duct diameter corresponding to the reference duct, i.e. M5FS, an improvement of the obtained results regarding noise reduction and aerodynamic properties of the fan can be assumed.

4.2. Fan blade skew and fan position

This subchapter is intended to clarify how the developed MPA duct affects the performance and sound radiation of different fans. In addition, it will be analysed which differences in the operating behaviour of the fan occur when the fan operates directly within the MPA duct section or downstream in a standard duct section.

Fig. 11 shows the aerodynamic and acoustic properties of a forward skewed fan (F) and a backward skewed fan (B). The two fans were investigated for the RFS and MFS variants, i.e. with free inflow and short duct (fan operates directly in the MPA duct section). The aerodynamic characteristics (Fig. 11(a)) show that both fans have a lower pressure build-up in the case of the MFS. This can be connected to the larger tip gap, as demonstrated in the previous chapter. This is also reflected in a loss of efficiency for both fans (Fig. 11 (b)). The noise reductions (Fig. (11(c)) take place for both fans over the entire characteristic curve. However, the largest reductions in sound pressure level take place with the backward skewed fan (B). In the unsteady range of the characteristic curve, the sound sources are more dominant in this fan than in the forward skewed fan due to tip gap flow interactions. This is caused by the different radial velocity components of the skewed fan blades [8,11,60]. The noise reduction assumes values of up to $\Delta L_p = 16$ dB for the backward skewed fan (B). The dominant peak in the characteristic curve can thus be attenuated and the acoustic characteristic curve of the fans is much flatter. This indicates that the sound radiation in relation to the total sound pressure level becomes more independent of the volume flow rate $\dot{V}$. As a result, the noise level of the ventilator appears more constant when changing volume flows occur in a system.

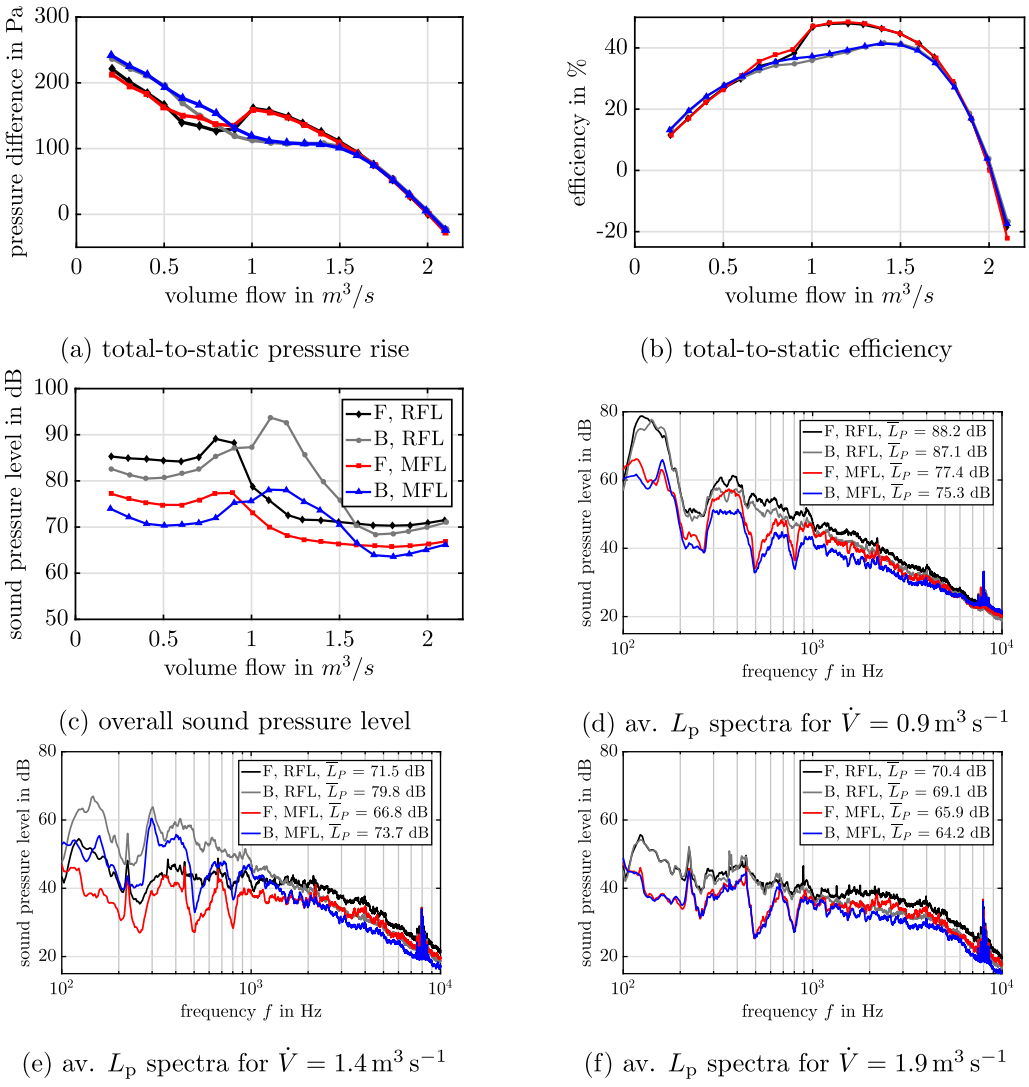

(a) total-to-static pressure rise

(b) total-to-static efficiency

(c) overall sound pressure level

(d) av. L_p spectra for $\dot{V} = 0.9\,\mathrm{m^3\,s^{-1}}$

(e) av. L_p spectra for $\dot{V} = 1.4\,\mathrm{m^3\,s^{-1}}$

(f) av. L_p spectra for $\dot{V} = 1.9\,\mathrm{m^3\,s^{-1}}$

Fig. 12. Aerodynamic and acoustic results for the comparison between the fans F and B in the long duct.

The sound pressure spectra show that the reductions are independent of the operating point of the fan in the frequency range up to $f = 2$ kHz. In the partial load range, both fans show a slight increase in the sound pressure spectra starting at $f = 3$ kHz. This could also be determined in the case of the M5FS from the previous chapter. From this it can be concluded that this high-frequency rise is the inherent noise of the MPA, which is produced when the air flows through and over the absorber. A similar high-frequency noise could be detected during the flow over and through porous wings in the wind tunnel, which were also used for sound absorption in the literature [61,62]. A similar inherent noise was also found by Nelson [63] in basic experiments, who covered the openings of the perforations with cloth to identify the influence of the noise of the openings. This noise is highly dependent on the pressure difference p_ts generated and the volume flow rate $\dot{V}$ applied. In the overload range, sound pressure level of the forward skewed fan (F), which generates higher sound pressure with regard to the sound sources on the trailing edge, is reduced by the MPA up to $f = 6$ kHz. At higher frequencies, this fan then experiences an increase of the emitted sound. The results allow the statement that the effects and interactions found between the MPA and the fan are basically applicable and transferable to different fans.

The next step is to investigate the interaction of the MPA with the two fans in the long duct version. In this variant, the duct was extended by one section and the fans operate behind the MPA in a standard duct section. The aerodynamic characteristics (Fig. 12(a)) clearly show that the MPA no longer has a negative effect on the pressure build-up. In the partial load range an increase of the generated pressure difference can even be generated. In the long version of the duct the effects of the tip gap dimensions are the same for the reference case as for the case with MPA. According to this, the MPA seems to have a positive influence on the aerodynamics of the fan in the partial load range. This positive effect is visible in the efficiency curve (Fig. 12(b)), which otherwise shows an identical course between reference case and MFL. In the case M5FS from the previous chapters, the tip gap between reference case and M5FS was also identical, but nevertheless the efficiency was reduced due to the MPA. Since this is no longer visible here, it can be concluded that when the fan operates directly within the MPA section, the small pores of the absorber cause a larger backflow from the pressure side to the suction side of the fan, which reduces the efficiency. If the fan operates downstream the MPA, within a standard duct segment, the backflow is unchanged compared to the reference case. Looking at the acoustic

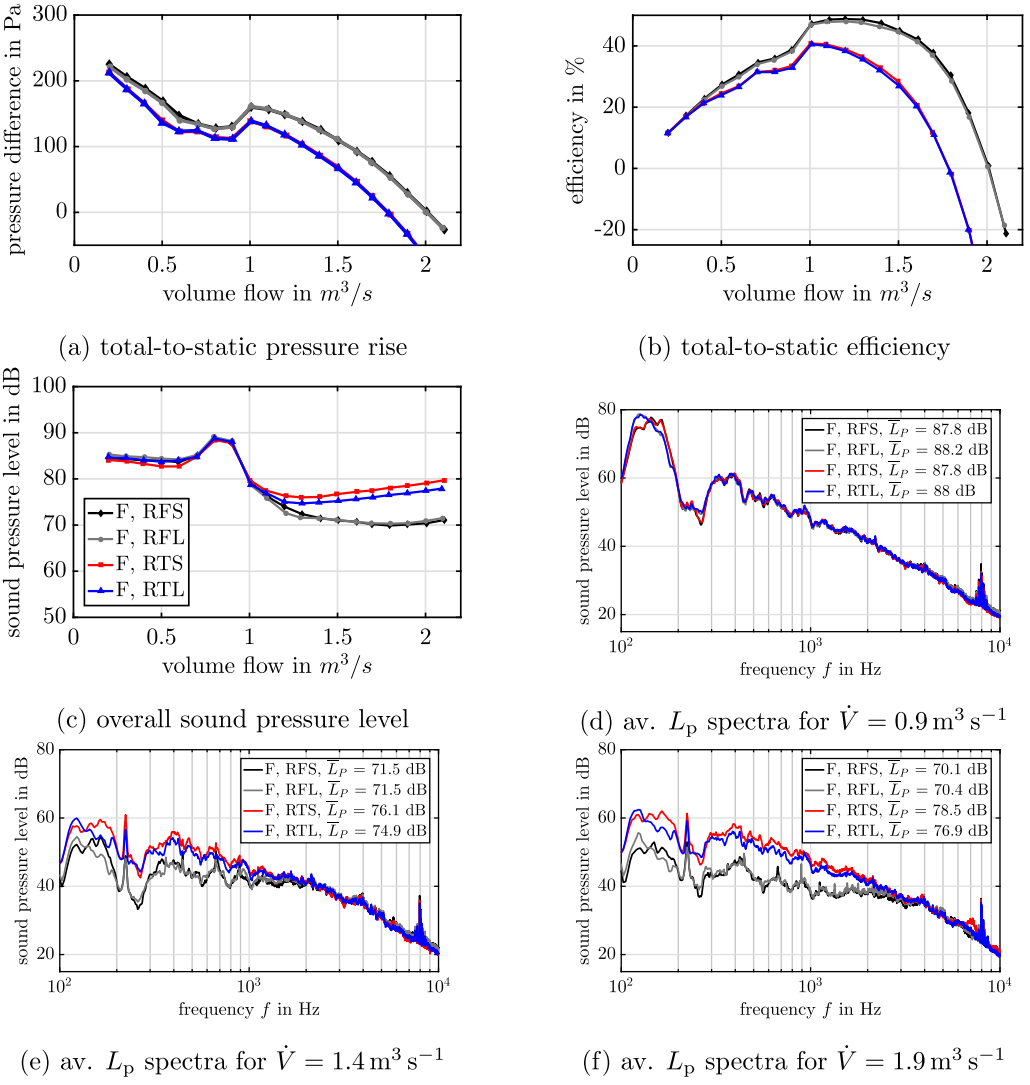

(a) total-to-static pressure rise

(b) total-to-static efficiency

(c) overall sound pressure level

(d) av. L_p spectra for $\dot{V} = 0.9\,\mathrm{m^3\,s^{-1}}$

(e) av. L_p spectra for $\dot{V} = 1.4\,\mathrm{m^3\,s^{-1}}$

(f) av. L_p spectra for $\dot{V} = 1.9\,\mathrm{m^3\,s^{-1}}$

Fig. 13. Influences of the turbulence grid on the aerodynamics and acoustics of fan F in the short and long reference duct.

characteristics (Fig. 12(c)), it can be seen that the sound radiation of the reference cases has changed only minimally due to the extension of the duct. The sound reductions caused by the MPA have been significantly increased compared to the MFS case with the short duct, although the effective absorber surface has remained the same. A reason could be that the absorber in the case of the long duct is no longer flowed through as strongly as in the short duct case. This is because the high-frequency component in the sound spectra (Fig. 12(d-e)), which is caused by the inherent noise of the absorbers through which the air flows, is no longer present.

The damping effects of the MPA are also limited over a larger frequency range up to $f = 7$ kHz in the partial load range and up to $f = 10$ kHz in the other operating points. The pronounced tonal components from the case with short duct are no longer visible in the sound pressure spectra. This indicates that these are due to the irregular weld seam of the MPA when the fan blade has moved over it. The frequencies of $f = 500$ Hz and $f = 800$ Hz are particularly significant in the sound pressure ranges, as these are where a strong noise reduction takes place. Summarising the obtained results from this chapter, it can be said that the variant with the long duct segment, in which the fan operates downstream of the MPA, is a more efficient variant in terms of noise reduction and aerodynamics. In addition, disturbing influences of the MPA such as inherent noise and blind flows can be reduced in this variant. All these findings are apply for both fan types.

4.3. Inflow conditions

This chapter discusses how a disturbed inflow affects the interaction between the fan and MPA. Both the long (L) and the short (S) variant are examined, whereby the disturbed inflow is generated via a turbulence grid (T). The forward skewed fan (F) is used for these investigations. This fan reacts more sensitively to a disturbed inflow than the backward skewed fan. In the first place, the effects of the turbulence grid are discussed on the basis of the reference cases.

The aerodynamic curves shown in Fig. 13(a) reflect the characteristics of the system (axial fan and installations). Accordingly, the pressure build-up is reduced by the turbulence grid, which represents an additional pressure loss in the system. This additional pressure loss is compensated by the auxiliary fan, so that for the same volume flow the fan operates at the same operating point with and without the grid. The acoustic characteristics show that the turbulence grid has an influence on the emitted sound pressure

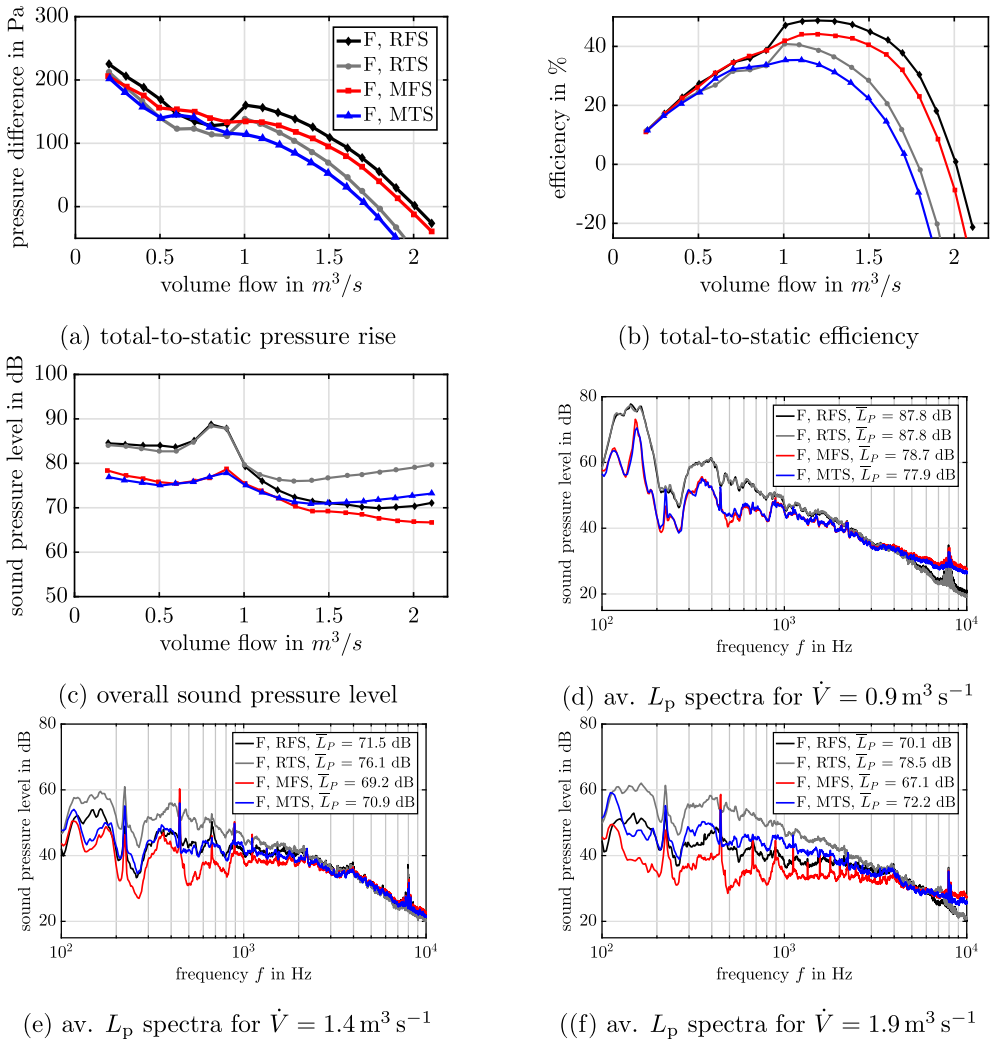

(a) total-to-static pressure rise (b) total-to-static efficiency

(c) overall sound pressure level (d) av. L_p spectra for $\dot{V} = 0.9\,\mathrm{m^3\,s^{-1}}$

(e) av. L_p spectra for $\dot{V} = 1.4\,\mathrm{m^3\,s^{-1}}$ ((f) av. L_p spectra for $\dot{V} = 1.9\,\mathrm{m^3\,s^{-1}}$

Fig. 14. Influences of the turbulence grid on the aerodynamics and acoustics of fan F in the short reference duct and the short MPA duct.

level starting at a volume flow rate of $\dot{V}$=1.0 $\mathrm{m^3\ s^{-1}}$. The sound pressure level of the fan increases by $\Delta L_\mathrm{p} = 6.5$ dB in the long duct and by $\Delta L_\mathrm{p} = 9$ dB in the short duct. From previous studies it can be assumed that the inherent noise of the turbulence grid only plays a minor role [11]. The sound pressure spectra (Fig. 13(d-e)) show that the increased inflow turbulence influences the sound pressure level of the fan up to a frequency of $f = 2$ kHz. For higher volume flow rates $\dot{V}$ this range increases up to $f = 3$ kHz. The increased sound generation mechanism can be assigned to the leading edge of the fan due to the low frequency range [64,65].

The next section deals with the influence of flow with increased turbulent kinetic energy on the short MPA duct. The inflow turbulence is generated by a upstream turbulence grid. This should clarify whether influences such as a disturbed inflow, which can be caused in real plants and systems for example by dripping protective grids or pipe redirection, have an effect on the absorbing properties of the MPA. In the short duct in which the fan operates directly in the vicinity of the MPA, the same effects of the MPA can be determined for both free and turbulent flow. This is reflected in the efficiency as well as the pressure build-up of the fan (Fig. 14(a and b)). However, the acoustic characteristic curve (Fig. 14(c)) shows that the damping properties of the MPA have been increased in the case of a turbulent inflow. This could be due to the fact that the overall sound pressure level was increased by the higher turbulence and the MPA absorbs better at a higher overall level. A further physical reason for the improved sound absorption properties of the MPA duct under turbulent inflow conditions could be that the increased turbulent kinetic energy also increases the fluctuation components of the flow perpendicular to the MPP surface. These additional fluctuations stimulate the air columns in the pores to oscillate further, which leads to higher dissipation inside the pores. Thus, the designed absorber counteracts a worsening of the flow and the resulting increased sound pressure level of the fan. In the case of turbulent inflow, a reduction of up to $\Delta L_\mathrm{p} = 6$ dB on the total sound pressure level can be achieved. In the case with free inflow this reduction was $\Delta L_\mathrm{p} = 4.5$ dB.

Similar observations can be made on the long duct variant with respect to the turbulence grid. The additional pressure build-up (Fig. 15(a)) which is caused by the MPA in the partial load range is also present with an installed turbulence grid. The reductions in the long duct variant turn out in the same order as before in the short duct variant. In case of a turbulent inflow the reduction is increased by $\Delta L_\mathrm{p} = 1.5$ dB compared to undisturbed inflow. The sound pressure spectra show dominant frequencies of $f = 500$ Hz and $f = 800$ Hz. The strong absorption at the two fre-

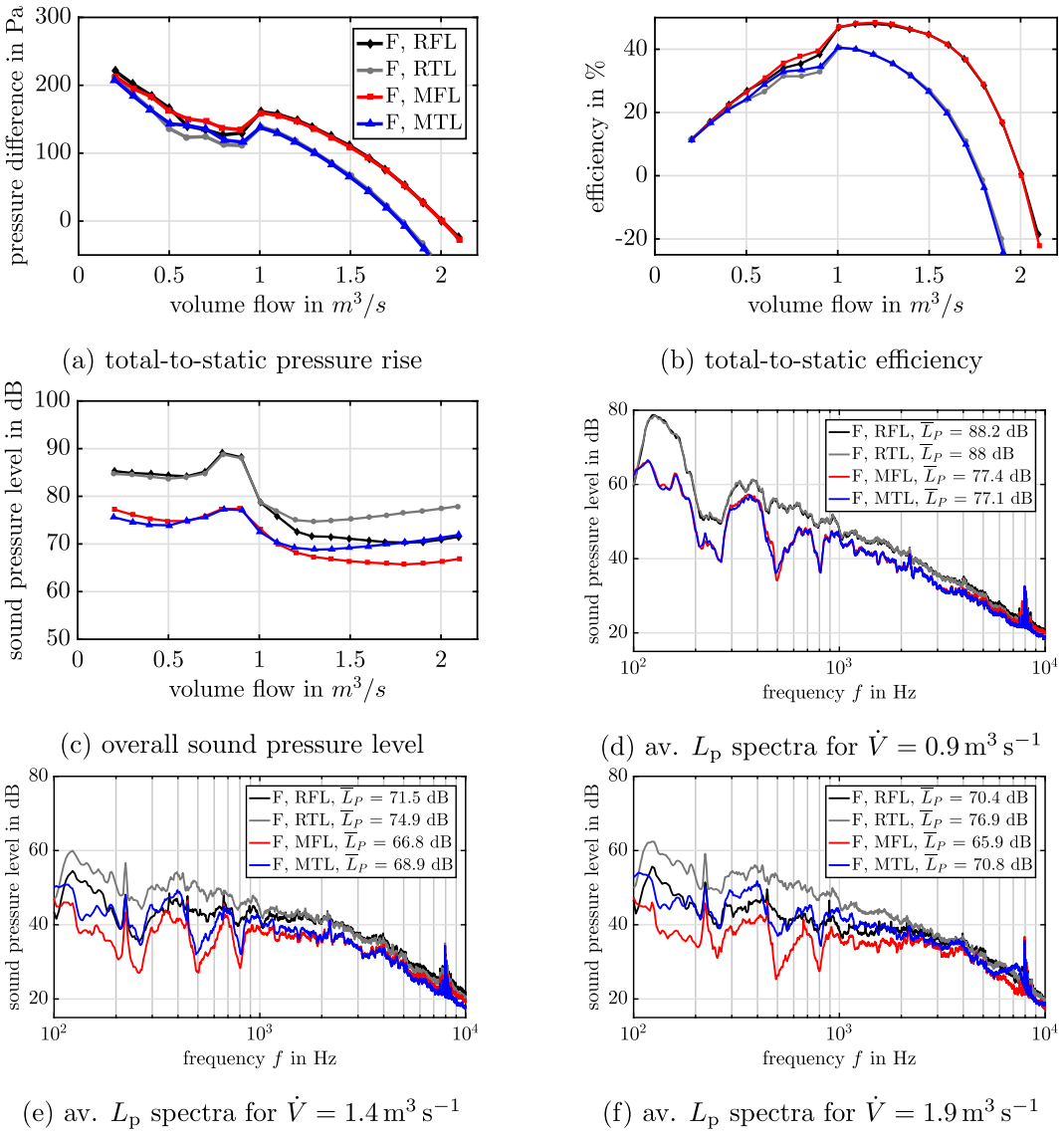

(a) total-to-static pressure rise

(b) total-to-static efficiency

(c) overall sound pressure level

(d) av. L_p spectra for $\dot{V} = 0.9\,\mathrm{m^3\,s^{-1}}$

(e) av. L_p spectra for $\dot{V} = 1.4\,\mathrm{m^3\,s^{-1}}$

(f) av. L_p spectra for $\dot{V} = 1.9\,\mathrm{m^3\,s^{-1}}$

Fig. 15. Influences of the turbulence grid on the aerodynamics and acoustics of fan F in the long reference duct and the long MPA duct.

quencies is pronounced for both the free and turbulent flow. In comparison to the short duct, the absorption is more intense in the long duct. The axial cavity length L_c is 440 mm, and therefore standing waves in the back volume can propagate at a frequency of $f = 780$ Hz. This resonator effect causes a strong reduction of the sound in this frequency range. The absorption at $f = 500$ Hz was selected as target frequency in the design process with CFS++. Absorption in this frequency range is due to the combined effect of the MPP and the cavity with a depth of $D_\mathrm{c} = 137$ mm.

5. Conclusion

In this study, a novel large scale duct absorber was presented and experimentally investigated. The investigations were carried out in a standardized axial fan test rig. The duct absorber consists of a micro-perforated plate (MPP), which is used for flow guiding. Behind this absorber a cavity is placed, which is supposed to increase the sound reduction by its impedance and diameter change. It was investigated how the new absorber affects the aerodynamics, performance and sound emission of different axial fans. Furthermore, different positions of the fan within in the MPA duct section and the impact of inflow turbulence were analyzed. The new findings from this study can be summarized as follows:

It could be shown that a micro-perforated absorber (MPA) can be used as a duct absorber. It was found that this absorber is suitable for flow guiding and does not strongly influence the aerodynamics and the efficiency of the fan compared to the reference case (standard duct) while the tip gap dimensions of the axial remain the same.

The micro-perforated sound absorber functions independently of the skew of the installed fan. A strong reduction of the emitted sound could be observed with a backward skewed fan. In most cases, a backward skewed fan has a higher sound pressure level of the sound sources in the tip gap region. This is particularly evident in the unsteady range of the characteristic curve. In this case, reductions of the sound pressure level of up to $\Delta L_\mathrm{p} = 16$ dB could be achieved with the designed micro-perforated duct absorber.

It has been shown that the efficiency and pressure build-up of the fan remain unaffected by the absorber when the fan operates downstream of the absorber in a standard duct section. This arrangement can prevent the flow from passing through the

micro-perforations of the absorber, thus increasing the backflow form the pressure side to the suction side of the axial fan. In addition, the sound attenuation properties of the absorber are more pronounced when the fan is located behind the absorber. If the fan operates within the duct section including the absorber, the radial components of the flow can cause the air to flow through the absorber openings, resulting in a high-frequency inherent noise of the absorber. The intensity of this inherent noise of the micro-perforated plate depends on the pressure difference p_{ts} and the volume flow rate $\dot{V}$.

It can be shown that inflow turbulence does not reduce the sound absorber effect of the MPA duct. The absorption properties of the micro-perforated duct absorber was increased with higher turbulence of the inflow. This could be due to the turbulent fluctuations perpendicular to the surface of the MPP being amplified, resulting in increased dissipation within the pores.

The absorbing effect of the duct silencer could be determined over a wide frequency range, which was in investigated cases at least up to $f = 2$ kHz. In addition, frequency ranges (around $f = 500$ Hz and $f = 800$ Hz) could be identified which showed a strong reduction of the sound pressure level. These frequency ranges can be influenced by the geometric properties of the absorber (length, cavity depth).

For the following investigations, further boundary conditions, such as the influences of a subdivision of the back volume, should be investigated. In order to better understand the development of the inherent noise when the microperforated absorber is flowed over and through, the influence should be clarified by basic experiments. On the basis of this study, it can be concluded that the modified concept of microperforated absorbers for the use in ducts of axial fans has proven to be a future-oriented approach. This concept reduces the noise of ventilation systems without aerodynamic pressure loss. The results of this investigation can be applied in further application scenarios, e.g. an installation of MPP in the area of the blade leading edge of axial fans could be a measure to reduce the noise emission of fans. An application of these absorbers in the area of the outlet of centrifugal fans would also be conceivable.

Declaration of Competing Interest

The authors declare that they have no known competing financial interests or personal relationships that could have appeared to influence the work reported in this paper.

CRediT authorship contribution statement

Felix Czwielong: Conceptualization, Software, Validation, Formal analysis, Investigation, Data curation, Writing - original draft, Writing - review & editing, Visualization. **Sebastian Floss:** Conceptualization, Software, Validation, Formal analysis, Investigation, Data curation, Writing - original draft, Writing - review & editing, Visualization. **Manfred Kaltenbacher:** Conceptualization, Software, Formal analysis, Resources, Writing - review & editing, Supervision, Project administration, Funding acquisition. **Stefan Becker:** Resources, Writing - review & editing, Supervision, Project administration, Funding acquisition.

Declaration of Competing Interest

The authors declare that they have no known competing financial interests or personal relationships that could have appeared to influence the work reported in this paper.

References

[1] Lu HZ, Huang L, So RMC, Wang J. A computational study of the interaction noise from a small axial-flow fan. J Acoust Soc Am 2007;122. https://doi.org/10.1121/1.2764474.
[2] Oktay Z. Testing of a heat-pump-assisted mechanical opener dryer. Appl Therm Eng 2003;23:153–62. https://doi.org/10.1016/S1359-4311(02)00112-6.
[3] Teitel M, Levi A, Zhao Y, Barak M, Bar-lev E, Shmuel D. Energy saving in agricultural buildings through fan motor control by variable frequency drives. Energy Build 2008;40:953–60. https://doi.org/10.1016/j.enbuild.2007.07.010.
[4] Cyrus V, Pelnar J, Cyrus J. Reversing of axial flow fans for ventilation. In: ASME 2011 turbo expo: turbine technical conference and exposition, GT2011-46062, ASME; 2011. p. 471–82.https://doi.org/10.1115/GT2011-46062..
[5] Lucius A, Schneider M, Bortoli SS-D, Gerhard T, Geyer T. Aeroacoustic simulation and experimental validation of sound emission of an axial fan applied in a heat pump. In: Proceedings of the 23rd international congress on acoustics DEGA-Akustik.
[6] Rynel A, Efraimsson G, Chevalier M, Abom M. Acoustic characteristics of a heavy duty vehicle cooling modul. Appl Acoust 2016;111:67–76. https://doi.org/10.1016/j.apacoust.2016.04.004.
[7] Becher M, Krusche R, Tautz M, Mauß M, Springer N, Krömer F, Becker S. Influence of the gap flow of axial vehicle cooling fans on radiated narrowband and broadband noise. Acta Acust United Acustica 2019;105:435–48. https://doi.org/10.3813/AAA.919326.
[8] Corsini A, Rispoli F. Using sweep to extend the stall-free operational range in axial fan rotors. Proc Inst Mech Eng Part A J Power Energy 2004;218129–39. https://doi.org/10.1243/095765004323049869..
[9] Carolus T, Beiler M. Skewed blades in low pressure fans: a survey of noise reduction mechanisms. In: Proceedings of 3rd AIAA/CEAS Aeroacoustics Conference, AIAA Paper 97-1591, Atlanta, USA; 1997. p. 47–53.https://doi.org/10.2514/6.1997-1591..
[10] Florian Z, Gert H, Stefan B. Acoustic characterization of forward-and backward-skewed axial fans under increased inflow turbulence. AIAA J 2017:1241–50. https://doi.org/10.2514/1.J055383.
[11] Krömer FJ. Sound emission of low-pressure axial fans under distorted inflow conditions. Doctoral thesis, FAU University Press; 2018.https://doi.org/10.25593/978-3-96147-089-1..
[12] Corsini A, Delibra G, Sheard AG. On the role of leading-edge bumps in the control of stall onset in axial fan blades. J Fluids Eng 2013;135:1–9. https://doi.org/10.1115/1.4024115.
[13] Roger M, Schram C, De Santana L. Reduction of airfoil turbulence-impingement noise by means of leading-edge serrations and/or porous materials. In: Proceedings of 19th AIAA/CEAS Aeroacoustics Conference, AIAA Paper 2013-2108, Berlin, Germany; 2013.https://doi.org/10.2514/6.2013-2108..
[14] Krömer F, Czwielong F, Becker S. Experimental investigation of the sound emission of skewed axial fans with leading-edge serrations. AIAA 2019;57. https://doi.org/10.2514/1.J058134.
[15] Czwielong F, Krömer F, Chaitanya P, Becker S. Experimental investigation of the influence of different leading edge modifications on the sound emission of axial fans downstream of a heatexchanger. In: Proceedings of the 23rd international congress on acoustics DEGA-Akustik.
[16] Ocker C, Geyer TF, Czwielong F, Krömer F, Becker S, Merkel M, Pannert W. Experimental investigation of the impact of 3d-metal-printed perforated leading edges on airfoil and axial fan noise. In: AIAA AVIATION 2020 FORUM. p. 2529. https://doi.org/10.2514/6.2020-2529.
[17] Krömer FJ, Renz A, Becker S. Experimental investigation of the sound reduction by leading-edge serrations in axial fans. AIAA J 2018;56:1–5. https://doi.org/10.2514/1.J056355.
[18] Biedermann T, Karmeier F, Paschereit C. Optimised test rig for measurements of aerodynamic and aeroacoustic performance of leading edge serrations in low-speed fan application. In: Proceedings of ASME Turbo Expo 2018 Turbomachinery Technical Conference and Exposition GT2018 GT2018-75369. ASME; 2018. https://doi.org/10.1115/GT2018-75369.
[19] Carolus T. Ventilatoren – Aerodynamischer Entwurf, Schallvorhersage, Konstruktion, 3rd ed., Springer Vieweg, Wiesbaden; 2013.https://doi.org/10.1007/978-3-8348-2472-1..
[20] Heinemann T, Becker S. Axial fan performance under the influence of a uniform ambient flow field. Int J Rotat Mach 2018. https://doi.org/10.1155/2018/6718750.
[21] Czwielong F, Krömer F, Becker S. Experimental investigations of the sound emission of axial fans under the influence of suction-side heat exchangers. In: 25th AIAA/CEAS Aeroacoustics Conference, volume AIAA 2019-2618 Session: Acoustic/Fluid Dynamics Interactions X; 2019.https://doi.org/10.2514/6.2019-2618..
[22] Stinnes W, von Backström T. Effect of cross-flow on the performance of air-cooled heat exchanger fans. Appl Therm Eng 2002;22:1403–15. https://doi.org/10.1016/S1359-4311(02)00060-1.
[23] Zenger FJ, Renz A, Becher M, Becker S. Experimental investigation of the noise emission of axial fans under distorted inflow conditions. J Sound Vib 2016;383:124–45. https://doi.org/10.1016/j.jsv.2016.07.035.
[24] Biedermann TM, Czeckay P, Hintzen N, Kameier F, Paschereit C. Applicability of aeroacoustic scaling laws of leading edge serrations for rotating applications. In: Acoustics, volume 2, Multidisciplinary Digital Publishing Institute; 2020. p. 579–94.https://doi.org/10.3390/acoustics2030030..

[25] Liu C, Ji Z, Fang Z. Numerical analysis of acoustic attenuation and flow resistance characteristics of double expansion chamber silencers. Noise Contr Eng J 2013;61. https://doi.org/10.3397/1/3761043.
[26] Möser M, Müller G. Handbook of engineering acoustics. Berlin Heidelberg: Springer-Verlag; 2013.https://doi.org/10.1007/978-3-540-69460-1..
[27] Liu J, Herrin D, Seybert A. Application of micro-perforated panels to attenuate noise in a duct (Technical Report). SAE Technical Paper; 2007.
[28] Allam S, Åbom M. A new type of muffler based on microperforated tubes. J Vib Acoust 2011;133. https://doi.org/10.1115/1.4002956.
[29] Fuchs H, Zha X. Acrylic-glass sound absorbers in the plenum of the deutscher bundestag. Appl Acoust 1997;51:211–7. https://doi.org/10.1016/S0003-682X(96)00064-3.
[30] Herrin D, Hua X, Liu J. Microperforated panel absorber design: a tutorial. In: 21st International congress on sound and vibration (ICSV21), Beijing, China; 2014. p. 13–7..
[31] Dong B, Xie D, He F, Huang L. Noise attenuation and performance study of a small-sized contra-rotating fan with microperforated casing treatments. Mech Syst Signal Process 147:107086.https://doi.org/10.1016/j.ymssp.2020.107086..
[32] Wang C, Huang L. On the acoustic properties of parallel arrangement of multiple micro-perforated panel absorbers with different cavity depths. J Acoust Soc Am 2011;130:208–18. https://doi.org/10.1121/1.3596459.
[33] Sakagami K, Oshitani T, Yairi M, Toyoda E, Morimoto M. An experimental study on a cylindrical microperforated panel space sound absorber. Noise Contr Eng J 2012;60:22–8. https://doi.org/10.3397/1.3670101.
[34] Lee Y, Lee E, Ng C. Sound absorption of a finite flexible micro-perforated panel backed by an air cavity. J Sound Vib 2005;287:227–43. https://doi.org/10.1016/j.jsv.2004.11.024.
[35] Floß S, Kaltenbacher M, Karlowatz G. Application and simulation of micro-perforated panels in hvac systems. In: Conference: 10th International Styrian Noise, Vibration & Harshness Congress: The European Automotive Noise Conference; 2019.https://doi.org/10.4271/2018-01-1514..
[36] Allam S, Abom M. Fan noise control using micro- perforated splitter silencers. J Vib Acoust 2014;136(3). https://doi.org/10.1115/1.4027245.
[37] Temiz MA, Tournadre J, Artega IL, Hirschberg A. Non-linear acoustictransferimpedanceofmicro-perforated plateswithcircularorifices. J Sound Vib 2016;366. https://doi.org/10.1016/j.jsv.2015.12.022.
[38] Zhang X, Cheng L. Acoustic impedance of micro-perforated panels in a grazing flow. J Acoust Soc Am 2019;145(2461). https://doi.org/10.1121/1.5098785.
[39] Lawn C. The acoustic impedance of perforated plates under various flow conditions relating to combustion chamber liners. Appl Acoust 2016;106. https://doi.org/10.1016/j.apacoust.2016.01.005.
[40] Floss S, Czwielong F, Krömer F, Becker S, Kaltenbacher1 M. Achieving axial fan sound reduction with micro-perforated absorbers. In: Fortschritte der Akustik – DAGA 2019 45. Deutsche Jahrestagung für Akustik, 18.-21. März 2019 in Rostock, DEGA-Akustik; 2019. p. 1410–3..
[41] Maa D-Y. Theory and design of microperforated panel sound-absorbing constructions. Sci Sin 1975;18:55–71. https://doi.org/10.1360/ya1975-18-1-55.
[42] Maa D-Y. Potential of microperforated panel absorber. J Acoust Soc Am 1998;104:2861–6.https://doi.org/10.1121/1.423870..
[43] Hua X, Herrin D, Jackson P. Varying backing cavity depths to achieve broadband absorption using micro-perforated panels. In: INTER-NOISE and NOISE-CON Congress and Conference Proceedings, volume 246, Institute of Noise Control Engineering; 2013. p. 841–8..
[44] Liu J, Hua X, Herrin D. Estimation of effective parameters for microperforated panel absorbers and applications. Appl Acoust 2014;75:86–93. https://doi.org/10.1016/j.apacoust.2013.07.009.
[45] Jaouen L, Bécot F-X. Acoustical characterization of perforated facings. J Acoust Soc Am 2011;129:1400–6. https://doi.org/10.1121/1.3552887.
[46] Kaltenbacher M. Numerical simulation of mechatronic sensors and actuators, vol. 2, Springer; 2007.https://doi.org/10.1007/978-3-642-40170-1..
[47] Kaltenbacher M, Floss S. Nonconforming finite elements based on nitsche-type mortaring for inhomogenous wave equation. J Theor Comput Acoust 2018;26:1850028-1–18.https://doi.org/10.1142/S2591728518500287..
[48] Krömer FJ, Becker S. Off-design sound emission of low-pressure axial fans under distorted inflow conditions: an experimental study. Acta Acust United Acustica 2019;105. https://doi.org/10.3813/AAA.919291.
[49] Herold G, Zenger F, Sarradj E. Influence of blade skew on axial fan component noise. Int J Aeroacoust 2017;16:418–30. https://doi.org/10.1177/1475472X17718740.
[50] Pfleiderer C. Strömungsmaschinen. Springer-Verlag; 2013.https://doi.org/10.1007/b138287..
[51] Carolus TH, Starzmann R. An aerodynamic design methodology for low pressure axial fans with integrated airfoil polar prediction. In: ASME 2011 Turbo Expo: Turbine Technical Conference and Exposition, American Society of Mechanical Engineers; 2011. p. 335–42.https://doi.org/10.1115/GT2011-45243..
[52] Kameier F, Neise W. Experimental study of tip clearance losses and noise in axial turbomachines and their reduction. J Turbomach 1997;119(3):229–43. https://doi.org/10.1115/1.2841145.
[53] Neise W, Michel U. Aerodynamic noise of turbomachines. Deutsche Forschungsanstalt für Luft-und Raumfahrt, eV, DLR, Institut für Strömungsmechanik, Abt. Turbulenzforschung, Berlin 5; 1994.https://doi.org/10.13140/2.1.3408.9760..
[54] Abbott IH, Von Doenhoff AE. Theory of wing sections, including a summary of airfoil data. Courier Corporation; 1959..
[55] I.O. f. S. DIN EN ISO 5801, Industrial fans-performance testing using standardized airways; 2007..
[56] Kameier F, Neise W. Rotating blade flow instability as a source of noise in axial turbomachines. J Sound Vib 1997;203:833–53. https://doi.org/10.1006/jsvi.1997.0902.
[57] Minniti III R, Blake W, Mueller T. Determination of inflow distortions by interpreting aeroacoustic response of a propeller fan. In: 4th AIAA/CEAS Aeroacoustics Conference. p. 2286. https://doi.org/10.2514/6.1998-2286.
[58] Wright T, Simmons W. Blade sweep for low-speed axial fans. J Turbomach 1990. https://doi.org/10.1115/1.2927413.
[59] Hanson DB. Spectrum of rotor noise caused by atmospheric turbulence. J Acoust Soc Am 1974;56:110–26. https://doi.org/10.1121/1.1903241.
[60] Yang L, Ouyang H, Du Z-H. Experimental research on aerodynamic performance and exit flow field of low pressure axial flow fan with circumferential skewed blades. J Hydrodyn Ser B 2007;19:579–86. https://doi.org/10.1016/S1001-6058(07)60156-5.
[61] Geyer TF, Sarradj E. Self noise reduction and aerodynamics of airfoils with porous trailing edges. In: Acoustics, volume 1, Multidisciplinary Digital Publishing Institute; 2019. p. 393–409.https://doi.org/10.3390/acoustics1020022..
[62] Geyer T, Sarradj E, Fritzsche C. Measurement of the noise generation at the trailing edge of porous airfoils. Exp Fluids 2010;48:291–308. https://doi.org/10.1007/s00348-009-0739-x.
[63] Nelson P. Noise generated by flow over perforated surfaces. J Sound Vib 1982;83:11–26. https://doi.org/10.1016/S0022-460X(82)80072-2.
[64] Krömer FJ, Moreau S, Becker S. Experimental investigation of the interplay between the sound field and the flow field in skewed low-pressure axial fans. J Sound Vib 2019;442:220–36.
[65] Wright S. The acoustic spectrum of axial flow machines. J Sound Vib 1976;45:165–223.